www.sciencemag.org/cgi/content/full/science.1234320/DC1

Supplementary Materials for

Observing Atomic Collapse Resonances in Artificial Nuclei on Graphene

Yang Wang, Dillon Wong,* Andrey V. Shytov, Victor W. Brar, Sangkook Choi, Qiong Wu, Hsin-Zon Tsai, William Regan, Alex Zettl, Roland K. Kawakami, Steven G. Louie, Leonid S. Levitov, Michael F. Crommie*

*Corresponding author. E-mail: crommie@berkeley.edu

Published 7 March 2013 on *Science* Express
DOI: 10.1126/science.1234320

This PDF file includes:

Materials and Methods
Supplementary Text
Figs. S1 to S10
Full Reference List

Materials and Methods

The experiments were performed using an Omicron LT-STM under ultra-high vacuum ($P < 10^{-10}$ Torr) at 5K. STM tips were calibrated against the Au(111) surface state before all measurements (*28*). Differential conductance (*dI/dV*) was measured by lock-in detection of the a.c. tunnel current modulated by a 6 mV (rms), 500-700 Hz signal added to the tunneling bias (V_s). The calcium getter (Alvatac) was first calibrated by evaporating Ca atoms into a mass spectrometer (Residual Gas Analyzer, SRS). The graphene sample was grown by the CVD method described in Ref. 15. Boron nitride flakes were exfoliated onto heavily doped silicon wafers coated by a 285nm thermal oxide. The graphene was placed on top of the BN / SiO_2 and electrical contact was made by depositing Ti (10-nm thick)/Au (30-nm-thick) electrodes using a stencil mask technique. Samples were annealed in UHV at T ~ 400 ^{o}C for several hours to clean them before loading into the STM. To prepare calcium dimers on graphene we first deposited calcium atoms from the calibrated getter source onto our graphene device while holding the graphene at low temperature (<10 K). Fig. S1A shows a representative STM topograph of the graphene surface at T=5K following a typical deposition of Ca and exhibits numerous individual Ca atoms (i.e., monomers). We then warmed the sample up to T=16 ± 3 K for 1 to 2 minutes before returning to T = 5K, thus causing the Ca adatoms to thermally diffuse and bind into dimers (we tested that this procedure does not result in contamination of the surface). Fig. S1B shows an STM topograph of Ca dimers prepared in this way on the graphene surface at T = 5K. Identification of dimers was verified by statistical analysis of the apparent height of 150 objects measured on random patches of graphene both before and after annealing the sample, which is summarized in the histogram in Fig. S1C. The histogram before annealing (blue) is dominated by one large peak (Ca monomers) while after annealing (red) the histogram clusters at three different heights (interpreted as monomer, dimer, trimer, and possibly larger Ca clusters, whose ratio can vary depending on the annealing temperature and the initial Ca-monomer

density before annealing). Similar dimerization behavior has been seen in other systems (*29, 30*). The parameters of pushing Ca dimers are V_s = -1 V, I = 2 pA and V_g = -60 V.

Supplementary Text

The effect of tip-induced band-bending

The effect of tip-induced band-bending (TIBB) is estimated by comparing the atomic collapse state peak energies in *dI/dV* spectra taken at the same lateral distance from a 5-dimer cluster, but with different tip-heights (Fig. S2). The range of current set points for the spectra shown in Fig. S2 corresponds to a total change in tip-height of 2Å (*20*). The peak energies extracted by fitting the quasi-bound state resonance in the range of 0.180eV < V_s < 0.250eV with a Lorentzian function are (0.213 ± 0.007eV) for I = 8pA, (0.215 ± 0.006eV) for I = 40pA, and (0.216 ± 0.004eV) for I = 500pA (the peak energy here is different than the one shown in Fig. 1E because this cluster has a slightly different geometric configuration). The fact that the atomic collapse state energy is insensitive to the tip-height (i.e., the energy shift is less than 2%) indicates that TIBB does not have a significant effect on our measurements of the atomic collapse state.

Method for Dirac equation simulation of graphene LDOS near a charged impurity

The theoretically simulated LDOS of graphene near a charged impurity is calculated using the same method as in Ref. 10. This Dirac equation simulation uses a 2D continuum model with linear dispersion for graphene, and the eigenstates are calculated for the Dirac equation under a Coulomb potential with a smooth cutoff at r_0 = 1nm (i.e., $V(r) = V(r_0)$ for $r < r_0$). The graphene electronic LDOS is then calculated using the eigenstate wavefunction expression. The simulated LDOS (before adding electron-phonon coupling and lifetime broadening) for Z/Z_c =0.5, 0.9, 1.4, 1.8 and 2.2 at the same distances away from the charge center as the experimental spectra near 1-5 Ca

dimer clusters are plotted in Figs. S3A to E. The effects of inelastic tunneling as well as lifetime broadening by electron-phonon and electron-electron interactions on the STM *dI/dV* spectra are included using the method of Ref. 21 to obtain the simulated *dI/dV* spectra of Figs. 1F-J. The fitted charge value for the 3-dimer cluster just passes the supercritical threshold, and the corresponding simulated LDOS (Fig. S3C) shows a peak due to the atomic collapse state that has small spectral intensity at the Dirac point. Because the LDOS surrounding this peak is highly asymmetric, the peak appears to be above the Dirac point after the lifetime broadening. This is an effect of the lifetime convolution (which is observed both in the experiment and in the simulation). The higher energy narrow peak at zero energy in the theoretical LDOS for a 5-dimer cluster (Fig. S3E) corresponds to the n=2 atomic collapse state with angular momentum of j=1/2 (*8, 9*). This peak becomes invisible after lifetime broadening (Fig. 1J) due to its small spectral weight, and so the experimental spectrum is dominated by the significantly higher spectral density of the lower energy n=1 state.

Dirac equation simulations using other values of the r_0 boundary condition

We have performed simulations for the experimental *dI/dV* spectra (Figs. 1A-E) around Ca-dimer clusters composed of 1-5 dimers using r_0 = 0.5nm (Figs. S4A-E) and r_0 = 1.5nm (Figs. S4K-O) to compare with the simulation using r_0 = 1.0nm showed in Figs. 1F-J (also plotted in Figs. S4F-J). Curves are shown for the Z/Z_c values that best fit the experimental data. The fact that both the resulting simulated spectra and the extracted Z/Z_c values are similar for simulations using different r_0 values indicates that r_0 is not a sensitive parameter for our simulation over the range 0.5nm $\leq r_0 \leq$ 1.5nm. Therefore we fix the value of r_0 to 1nm for all of our calculations in the paper since this is close to the geometry of our Ca dimer clusters. Variations in the fitted Z/Z_c values over the range 0.5nm $\leq r_0 \leq$ 1.5nm are accounted for in the Z/Z_c uncertainty values mentioned in the paper.

Spatial dependence of the atomic collapse state intensity

The radially averaged normalized *dI/dV* linescan measured at the atomic collapse state energy (V_s = +0.20V, V_g = -30V) around a 5-dimer cluster is plotted as a black solid line in Fig. S5. The lateral distance is measured from the cluster center. The corresponding simulation of the normalized *dI/dV* linescan using the same method that generates the spectra in Fig. 1J is plotted as a red dashed line in Fig. S5. The experimentally measured spatial dependence of the atomic collapse state intensity qualitatively matches the theoretical simulation, but there is some quantitative disagreement (the experimental peak decays more quickly with distance). The fact that the measured atomic collapse state intensity decays faster in distance than the theoretical prediction is possibly due to free-electron screening effects (*23, 24*) which are not included in the theory.

Normalized *dI/dV* spectra near a single Ca dimer at different back-gate voltages

Normalized *dI/dV* spectra taken around a single Ca dimer with back-gate voltages Vg = -60V, 0V and +30V are plotted in Fig. S6A, B and C respectively. At all of these back-gate voltages the normalized spectra display the typical asymmetric electron-hole behavior of a subcritical impurity (*14*), demonstrating that the Ca dimer is positively charged on graphene for the doping range of our study.

***Ab initio* calculation of the screened charge associated with a single Ca dimer on an isolated graphene sheet, as well as estimation of Z/Z_c associated with a single Ca dimer on graphene placed on a BN substrate.**

Z/Z_c associated with a single Ca dimer deposited on graphene placed on a BN substrate was estimated using *ab initio* density functional theory (DFT) techniques in the following ways. First, we calculated the screened charge associated with a single Ca dimer on isolated graphene, as seen by a test charge at large distance, using three different

methods (described below). All three methods arrived at the same value of a positively charged center missing 0.4 electrons as compared to a neutral Ca dimer. Then the dielectric screening from a BN substrate was incorporated. The additional substrate screening reduces the overall screened charge, resulting in a Z/Z_c associated with a single Ca dimer on graphene on a BN substrate estimated to be 0.6 ± 0.3, with $Z_c = \frac{\hbar v_F}{2e^2} = 0.25$.

As charges are transferred from a Ca dimer into graphene band states as carriers, the Ca dimer becomes charged and the electrons in the graphene layer self-consistently rearrange to screen the bare charge on the dimer. We computed the charge density around a calcium dimer on an isolated graphene sheet in the relaxed geometry obtained using the first-principles norm-conserving pseudopotential density functional theory (DFT), as implemented in the OpenMX package (*31*) which is based on a linear combination of pseudo-atomic orbital (LCPAO) method. The system is modeled by an n×n (n=8, 9, and 10) hexagonal graphene supercell with a Ca dimer as shown in Fig. S7. The in- and out-of-graphene plane lattice constants are n×2.47 Å and 1000 Å, respectively. The Brillouin zone is sampled with a 3×3×1 Γ-centered k-point grid and the wavefunction cutoff used is 150Ry. In the calculated relaxed structure in the generalized gradient approximation to the exchange correlation functional, both Ca atoms are located at 2.4 Å above the graphene plane with a Ca-Ca distance of 3.4 Å and the center of the Ca dimer is on the center of a C-C bond in graphene as shown in Fig. S7.

Partitioning the electron density in real space was used to evaluate the screened charge of the Ca dimer as seen by a test particle far from the dimer on an isolated graphene sheet. First, we defined the electron density difference, quantifying the redistribution of the electron density due to the dimer-graphene interaction, as

$$\Delta\rho(\mathbf{r}) = \rho_{ca+g}(\mathbf{r}) - \rho_g(\mathbf{r}) - \rho_{ca}(\mathbf{r}),$$

where $\rho_{ca+g}(\mathbf{r})$ is the electron density of the combined dimer-graphene system, and

$\rho_g(\mathbf{r})$ and $\rho_{ca}(\mathbf{r})$ are the electron density of an isolated graphene and an isolated Ca dimer in the same position as for the dimer-graphene system, respectively. Fig. S8 shows the z-direction-integrated charge density differences, $\Delta\bar{\rho}(x,y) = \int dz\, \Delta\rho(\mathbf{r})$. The electron density within a stadium-shaped region (a rectangle with a length of the Ca-Ca distance and a width of $2\times r_{sn}$ plus semicircles with a radius of r_{sn} on two sides) with the radius of r_{sn}, marked by black line in Fig. S8, redistributes the most. The net electron accumulation density outside the stadium-shaped region of radius r_{sn} is due to the electron transferred from the Ca dimer to the graphene itinerary states, which is expected to decrease to zero in the infinite supercell size limit. We estimated the screened charge on a Ca-dimer as seen by a test charge at large distance by calculating the integrated $\Delta\bar{\rho}(x,y)$ (or the monopole charge) in a stadium-shaped region. The radius of the particular stadium r_{sn}, that gives the screened charge associated with a dimer, is defined in our calculation as the radius r_s at which the net charge inside the region has a maximum value in magnitude, which is expected for a single Ca dimer on an infinitely extended pristine graphene sheet. Fig. S9 shows the net charge as a function r_s in our n×n graphene supercell calculation with n=8, 9, and 10, using the generalized gradient approximation to the exchange correlation functional. Around $r_s = 3.5\mathring{A}$, the net charge is at its maximum value in magnitude of -0.4*e*, where *e* is the electron charge (*e* = -|*e*|), from all three supercell calculations regardless of the exchange correlation functional used. As r_s increases to the supercell size dimension, the calculated net charge within the stadium in our calculations converges to 0 due to the finite supercell size used and charge neutrality condition. Uncertainty in the value of the screened charge as evaluated here originates from the finite supercell size and imposed charge neutrality condition, and should roughly be given by the ratio of the stadium area to the supercell area; in the case

of a 10x10 supercell, it should be approximately 10%.

In a second approach, we estimated the screened charge associated with a Ca dimer on an isolated graphene sheet by employing another widely used method of "real space partition" (*32*). The charge density was partitioned into two regions, one belonging to graphene and one to the Ca dimer. The position of the partitioning plane, which is parallel to the graphene plane (gray line in Fig. S10), is defined as the position at which the region of charge depletion changes to that of charge accumulation for charge transfer from the dimer to the graphene, as calculated from the x-y planar integrated electron density difference, $\Delta\tilde{\rho}(z) = \int dxdy\, \Delta\rho(\mathbf{r})$, as shown in Fig. S10 for the case of n=10. The screened charge associated with the Ca dimer is defined in this method by integrating $\Delta\tilde{\rho}(z)$ within the dimer region. This method also gives a screened charge value of -0.4*e* associated with the Ca dimer.

As a third method, the screened charge of a Ca dimer on an isolated graphene sheet was obtained by calculating the dipole moment of the graphene-dimer system along the graphene surface normal (out-of-plane) direction. By calculating the out-of-plane dipole moment of the system and knowing the separation between the Ca dimer and the graphene plane, we also obtain a screened charge value of -0.4*e* associated with the Ca dimer.

Our *ab initio* calculated results (from the three methods above and with three different supercell sizes) thus all give a screened charge of -0.4*e* associated with a single Ca dimer on an isolated graphene sheet. This value is insensitive to the particular exchange correlation functional used in our DFT calculation.

The dielectric screening from the BN substrate was incorporated next. This dielectric screening renormalizes the bare Coulomb interaction in graphene, so that the dielectric constant of isolated graphene (ϵ_g) will be renormalized (*24*) and the total dielectric constant of the dimer-graphene placed on the BN substrate may be represented as the

product of the renormalized dielectric constant of graphene ($\tilde{\epsilon}_g$) and the dielectric constant of the BN substrate (ϵ_s) within random phase approximation to the longitudinal polarizability. The screened charge of a single Ca dimer on graphene placed on a BN substrate is thus given by $Z = \frac{(-0.4e)\times\epsilon_g}{\tilde{\epsilon}_g \times \epsilon_s}$, where ϵ_g = 3 ± 1 (*23, 24, 33, 34*), $\tilde{\epsilon}_g$ = 3.0 ± 1.0 (*14*), and $\epsilon_s = 2.5 \pm 0.5$ (*16, 35, 36*). ϵ_g given here has a range of values depending on the method from which it is estimated. From *ab initio* calculation (*34*) at wavevectors relevant to this experiment its value is 2 to 4, while from a random phase approximation calculation (*23, 24*) $\epsilon_g \approx 4$, and an experimental (*33*) measurement puts it at $\epsilon_g \approx 2.2$. The uncertainty in $\tilde{\epsilon}_g$ arises from fitting experimental data to a Dirac model calculation (*14*), while uncertainty in ϵ_s comes from different reported values of the dielectric constant of BN (*16, 35, 36*) ($\epsilon_s = \frac{1+\epsilon_{BN}}{2}$). By taking into account the uncertainty of the screened charge of a single Ca dimer on isolated graphene in our calculation, as well as uncertainty in the different dielectric constants, a resulting Z/Z_c = 0.6 ± 0.3 for a single Ca dimer on graphene placed on a BN substrate is obtained (here $Z_c = \frac{\hbar v_F}{2e^2} = 0.25$ is the supercritical charge threshold).

<u>Comparison between the atomic collapse state in graphene impurities and in isolated 3D supercritical atoms</u>

Several theoretical studies (*8-10*) have demonstrated that supercritical impurities in graphene should show essentially the same atomic collapse physics as isolated 3D supercritical atoms. However, there are some subtle differences between the two cases, which we discuss below.

One such difference is the expression for the critical charge threshold, Z_c. Solving the 3D massive Dirac equation for the point charge Coulomb potential of an isolated atom

results in a ground state energy that becomes imaginary when $Z > \frac{1}{\alpha} \sim 137$, where α is the fine structure constant. However, Pomeranchuk and Smorodinsky (*2*) (among others) noticed that this conclusion is unphysical. They demonstrated that the singularity is eliminated if one introduces a cutoff in the potential. The true singularity occurs only when the level is pulled all the way through the mass gap. For a realistic nuclear radius this gives the critical charge threshold $Z_c \sim 170$.

For graphene charged impurities $Z_c = \frac{\hbar v_F}{2e^2} = \frac{1}{2\alpha_g} \sim 0.25$, where v_F is the graphene Fermi velocity and α_g is the graphene effective fine structure constant (*8, 9, 37*). Compared to the case for isolated 3D atoms, the expression of Z_c in graphene has an extra factor of 1/2. The origin of this extra factor is the 2D nature of graphene as shown in ref. 25. A simple, qualitative explanation can be made using the following semi-classical argument. Electrons in graphene have spin and so their dynamics are described by a Berry phase which is equal to π. One must account for this phase by including it in the Bohr-Sommerfeld rule for orbital angular momentum quantization:

$\oint p_\phi d\phi = 2\pi L = (2\pi m + \pi)\hbar$, where L is the angular momentum and m is an integer. The dynamics are thus effectively described by assigning L half-integer values. Atomic collapse occurs for small angular momentum: $|L| v_F < Ze^2$ (This follows from an analysis of classical trajectories, see, e.g., Landau and Lifshitz, *The Classical Theory of Fields*, Section 39). Using the lowest possible value of $L = \frac{1}{2}\hbar$ we arrive at

$$Z_c = \frac{\hbar v_F}{2e^2} = \frac{1}{2\alpha_g}.$$

Another difference between graphene charged impurities and isolated atoms is that for isolated atoms the subcritical regime exhibits "normal" Bohr-type bound states (due to finite electron mass) while electrons around subcritical impurities in graphene are completely delocalized (due to the zero effective mass of graphene charge carriers).

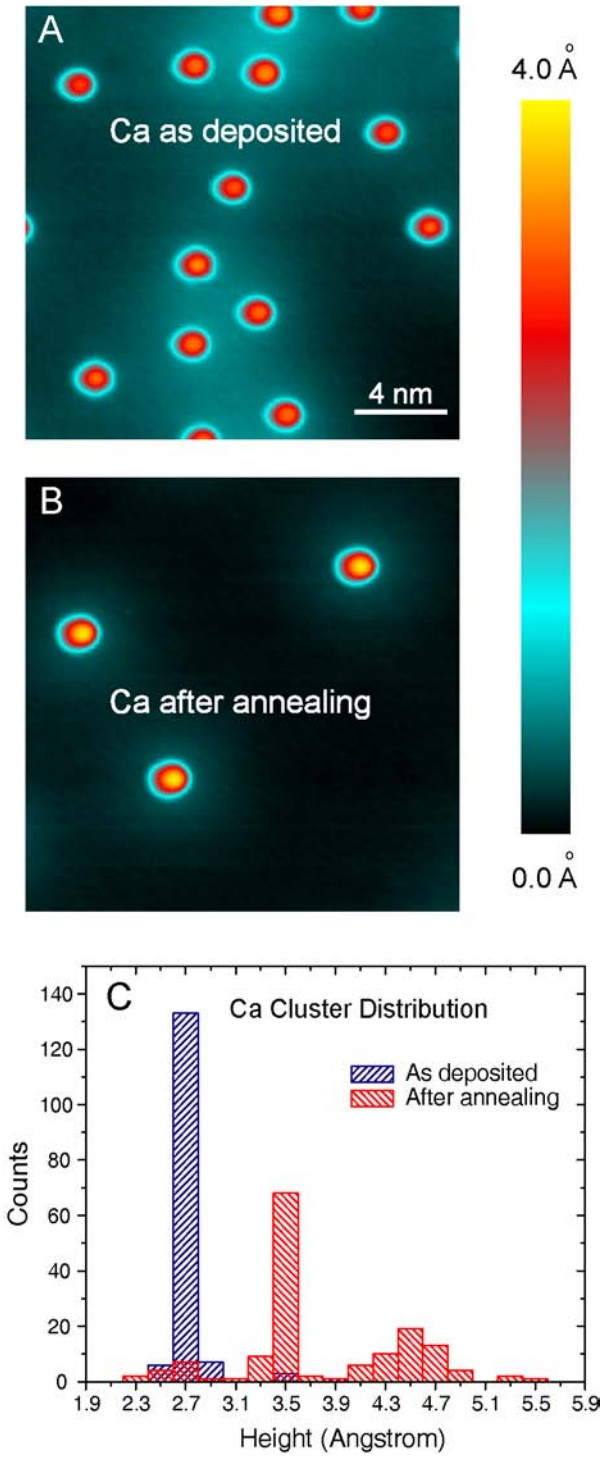

Fig. S1. (A) 18.8nm x 18.8nm STM topograph of the graphene surface at T = 5K following a typical Ca deposition shows Ca monomers (tunneling parameters: V_s= +0.30V, I=2pA). **(B)** Same size area at T = 5K after warming to T = 16K shows Ca

dimers (tunneling parameters: V_s= +0.40V, I=3pA). **(C)** Histogram of the apparent height of 150 objects measured on random patches of graphene at T = 5K both before (blue) and after (red) annealing to 16K.

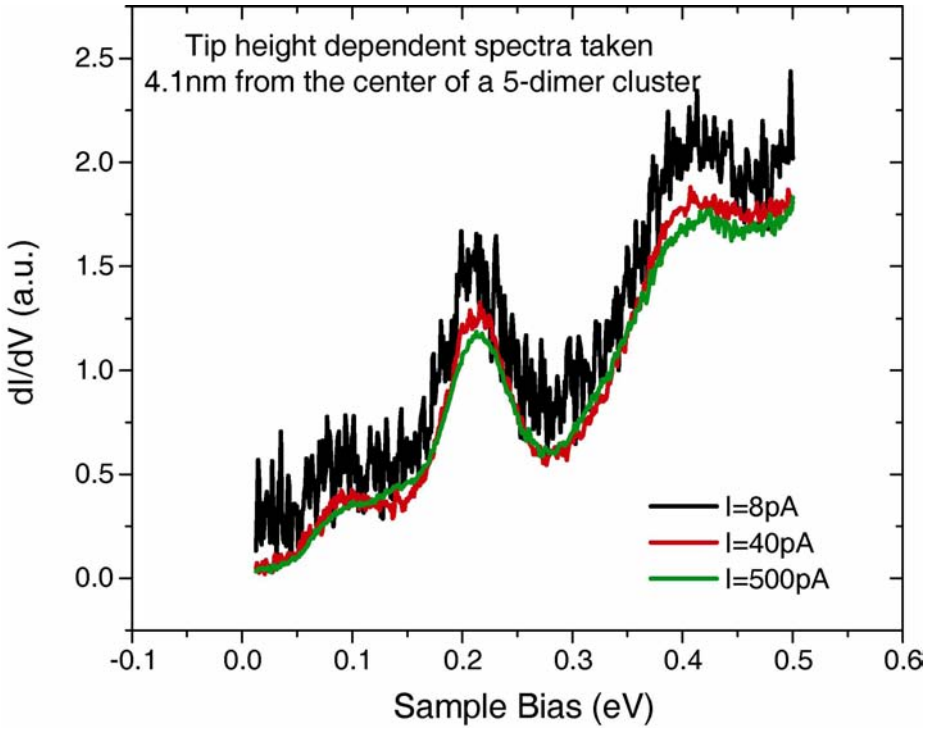

Fig. S2. *dI/dV* spectra taken 4.1nm from the center of a 5-dimer cluster using different set-point currents to test for tip-induced band-bending effects. No significant band-bending effects are observed. Initial tunneling parameters: V_s = +0.50V, I = 8pA, wiggle voltage V_{rms} = 6mV (black); V_s = +0.50V, I = 40pA, wiggle voltage V_{rms} = 6mV (red); and V_s = +0.50V, I = 500pA, wiggle voltage V_{rms} = 2mV (green). V_g = -30V for all measurements.

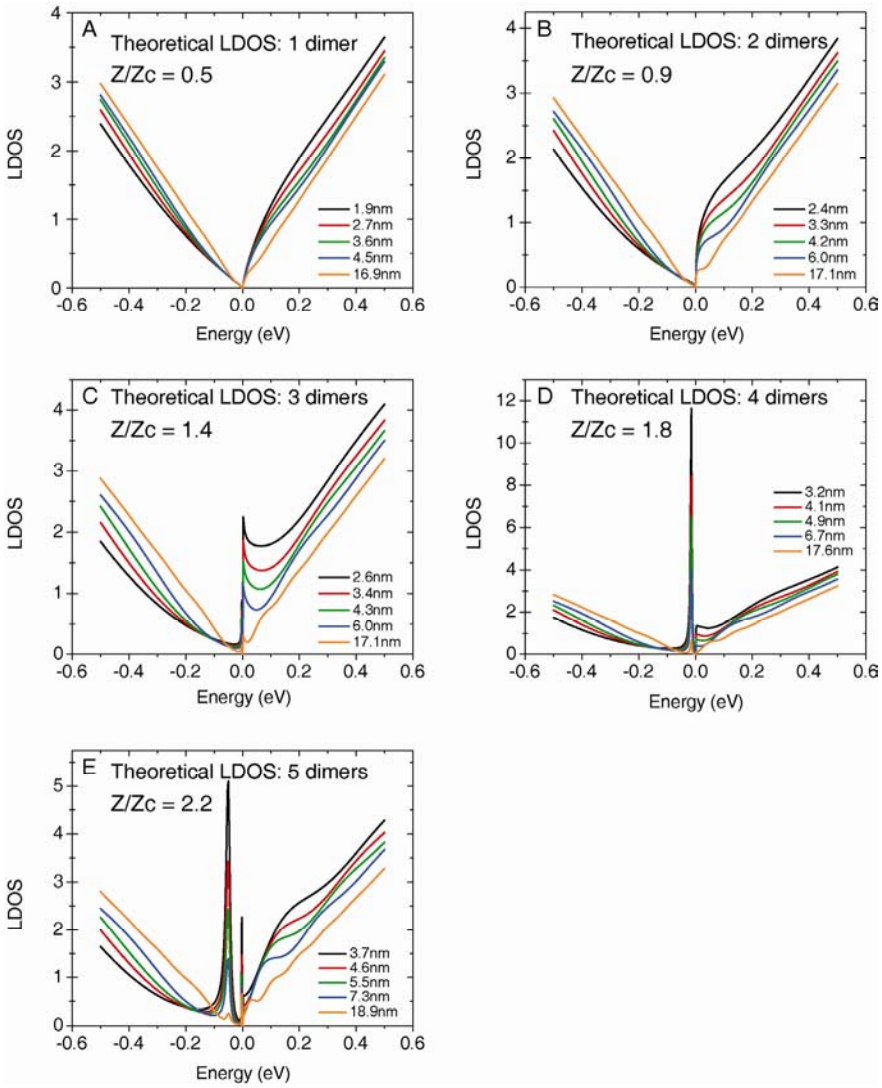

Fig. S3. Theoretical LDOS of graphene before adding inelastic tunneling and lifetime broadening. These curves are calculated using the Dirac equation for different distances from an impurity having charge of **(A)** $Z = 0.5Z_c$, **(B)** $Z = 0.9Z_c$, **(C)** $Z = 1.4Z_c$, **(D)** $Z = 1.8Z_c$, and **(E)** $Z = 2.2Z_c$ (Z_c is the critical charge threshold described in the text of the paper). The effects of inelastic tunneling and lifetime broadening must be added to the LDOS to simulate actual STM *dI/dV* spectra (as shown in Fig. 1 of the paper).

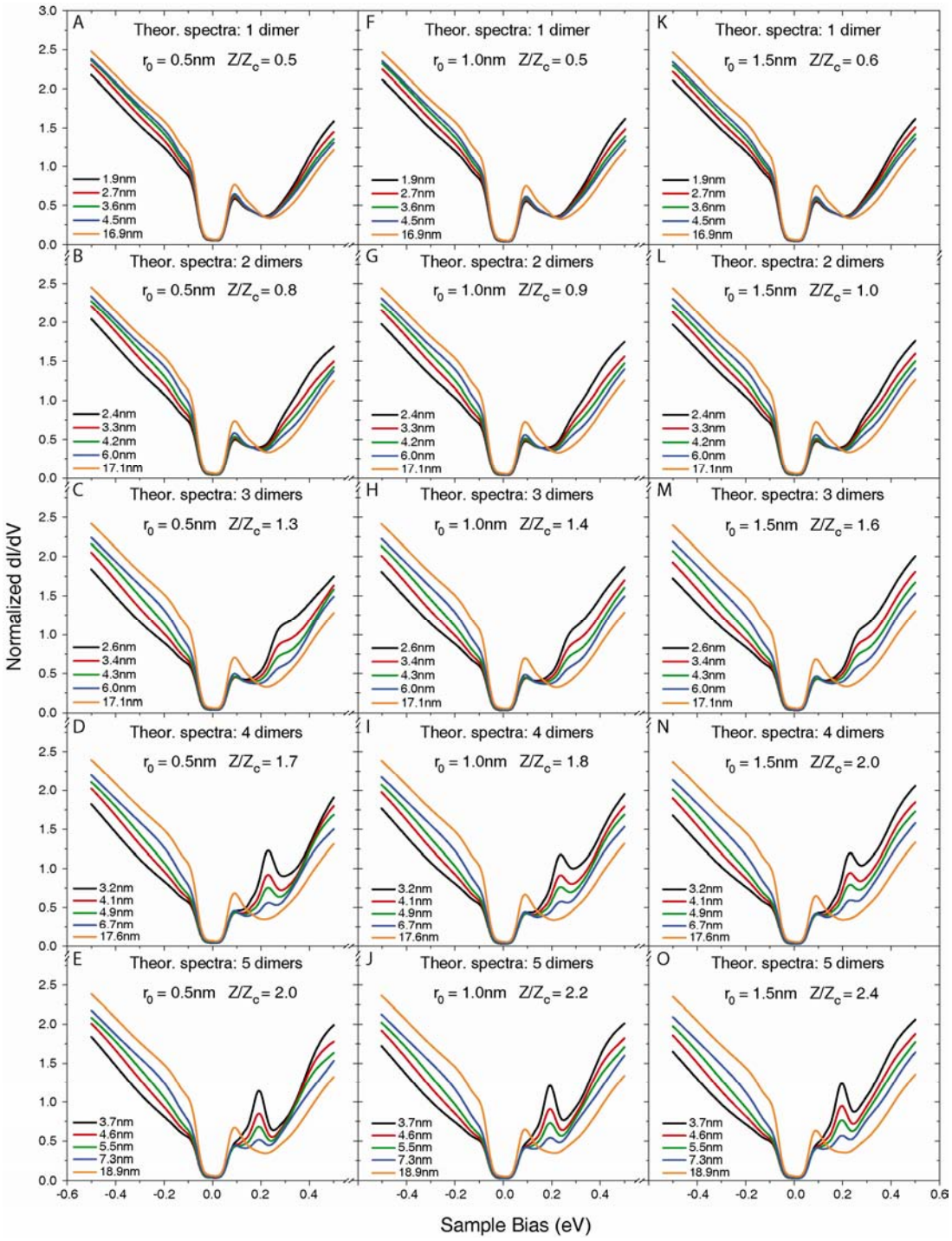

Fig. S4. (A-E) Theoretical normalized *dI/dV* spectra for graphene at different distances from the center of Ca-dimer clusters (i.e., artificial nuclei) composed of 1-5 dimers using boundary condition of $r_0 = 0.5$nm. **(F-J)** Theoretical normalized *dI/dV* spectra for

graphene at same distances as in **(A-E)** using boundary condition of r_0 = 1.0nm. **(K-O)** Theoretical normalized *dI/dV* spectra for graphene at same distances as in **(A-E)** using boundary condition of r_0 = 1.5nm. The best-fit Z/Z_c values are labeled in the figure.

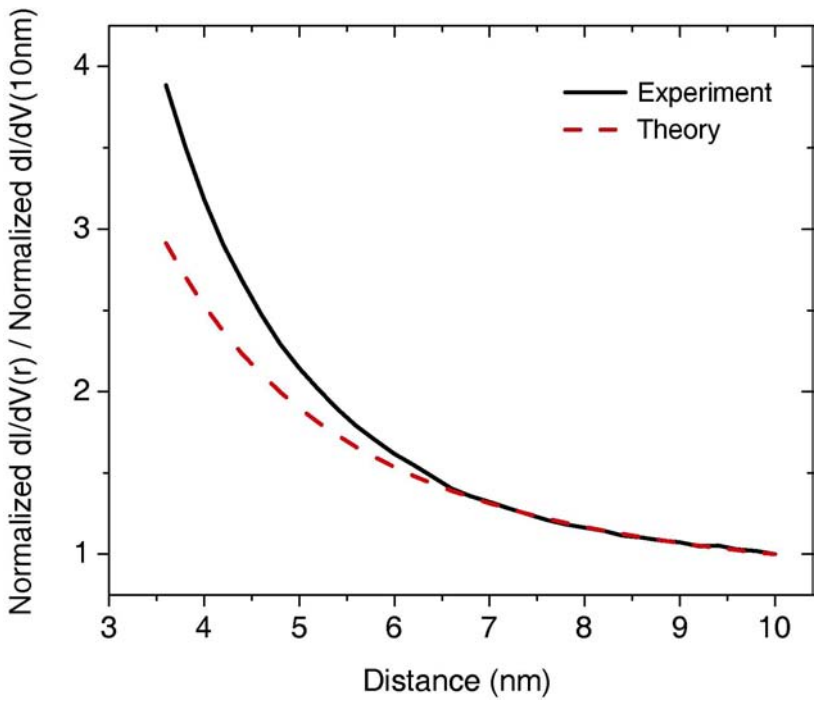

Fig. S5. Comparison between experimental and simulated distance dependence of the atomic collapse state intensity. Black solid curve: experimental radial averaged normalized *dI/dV* linescan for graphene as a function of lateral distance from the center of a 5-dimer cluster (tunneling parameters: V_s = +0.20V, I = 0.015nA, V_g = -30V, wiggle voltage V_{rms} = 6mV). Red dashed curve: theoretical simulated distance-dependent normalized *dI/dV* linescan for graphene near a charged impurity having $Z = 2.2Z_c$. Both curves are normalized by their value at r = 10nm.

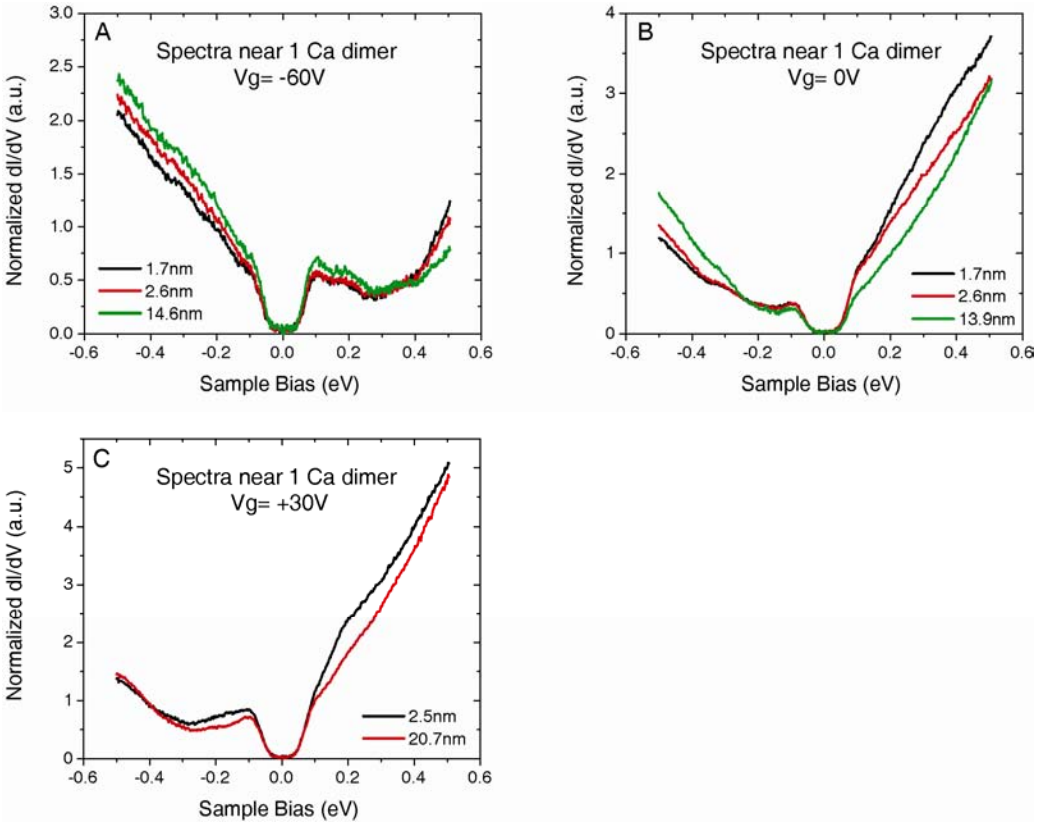

Fig. S6. Normalized *dI/dV* spectra taken at different distances away from a single Ca dimer on graphene for different gate voltages: **(A)** Vg = -60V, **(B)** Vg = 0V and **(C)** Vg = +30V. (Initial tunneling parameters: V_s = -0.50V, I = 0.06nA, wiggle voltage V_{rms} = 6mV)

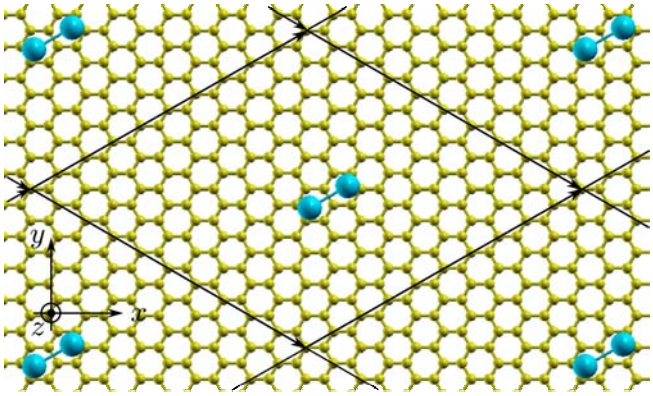

Fig. S7. Geometrical structure for a single Ca dimer on a 10×10 hexagonal graphene supercell used in *ab initio* DFT calculation.

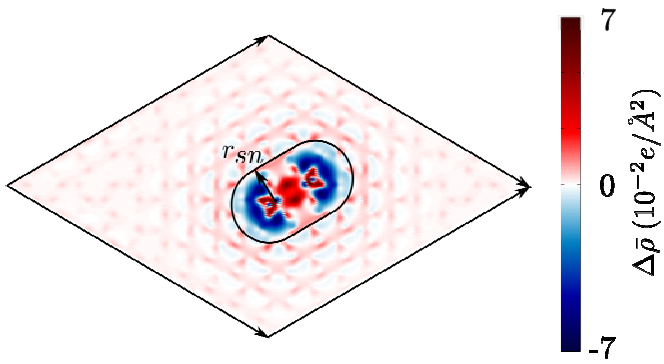

Fig. S8. Z-direction-integrated charge density difference $\Delta\bar{\rho}(x,y)=\int dz\,\Delta\rho(\mathbf{r})$ in a 10×10 hexagonal graphene supercell calculation. The stadium-shaped region (a rectangle with a length of the Ca-Ca distance and a width of $2\times r_{sn}$ plus semicircles with radii of r_{sn} on two sides) containing maximum net charge of -0.4*e* is shown by a black line.

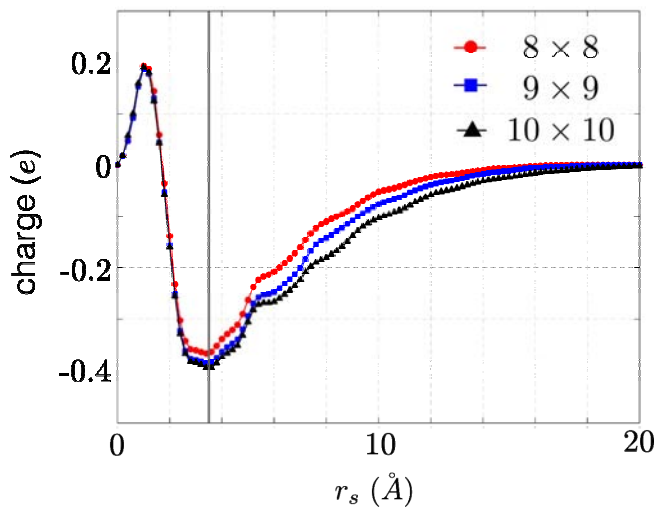

Fig. S9. The net charge inside a stadium-shaped region as a function of the stadium radius r_s calculated in the n×n hexagonal graphene supercell with n=8, 9, and 10. The particular stadium radius r_{sn} that gives the screened charge associated with the Ca dimer in our calculation is marked by a gray vertical line.

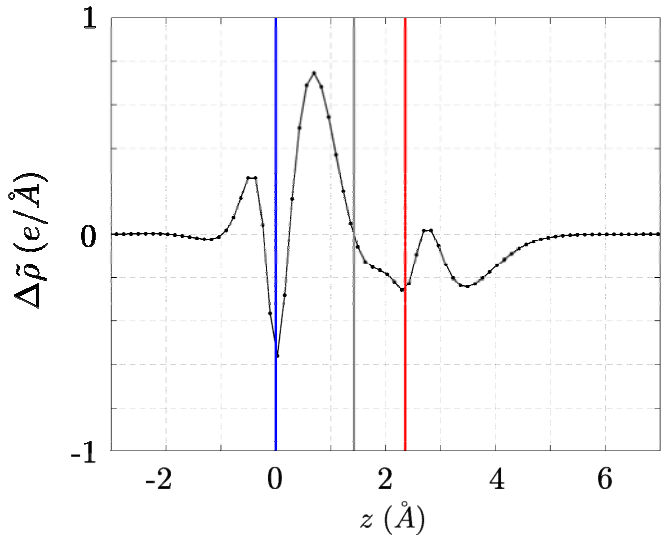

Fig. S10. The x-y planar integrated electron density difference $\Delta\tilde{\rho}(z) = \int dxdy\, \Delta\rho(\mathbf{r})$ as a function of the position along the out-of graphene plane direction. Blue, gray, and red vertical lines indicate the positions of the graphene sheet, the partition plane (see text), and the Ca dimer, respectively.

References and Notes

1. W. Greiner, B. Muller, J. Rafelski, *Quantum Electrodynamics of Strong Fields* (Springer, Berlin, 1985).

2. I. Pomeranchuk, Y. Smorodinsky, About the energy levels of systems with Z > 137. *J. Phys. USSR* **9**, 97 (1945).

3. Y. B. Zeldovich, V. S. Popov, Electronic structure of superheavy atoms. *Sov. Phys. Usp.* **14**, 673 (1972). doi:10.1070/PU1972v014n06ABEH004735

4. C. G. Darwin, On some orbits of an electron. *Philos. Mag. Ser. 6* **25**, 201 (1913). doi:10.1080/14786440208634017

5. T. H. Boyer, Unfamiliar trajectories for a relativistic particle in a Kepler or Coulomb potential. *Am. J. Phys.* **72**, 992 (2004). doi:10.1119/1.1737396

6. T. Cowan *et al*., Anomalous positron peaks from supercritical collision systems. *Phys. Rev. Lett.* **54**, 1761 (1985). doi:10.1103/PhysRevLett.54.1761 Medline

7. J. Schweppe *et al*., Observation of a peak structure in positron spectra from U+Cm collisions. *Phys. Rev. Lett.* **51**, 2261 (1983). doi:10.1103/PhysRevLett.51.2261

8. V. M. Pereira, J. Nilsson, A. H. Castro Neto, Coulomb impurity problem in graphene. *Phys. Rev. Lett.* **99**, 166802 (2007). doi:10.1103/PhysRevLett.99.166802 Medline

9. A. V. Shytov, M. I. Katsnelson, L. S. Levitov, Atomic collapse and quasi-Rydberg states in graphene. *Phys. Rev. Lett.* **99**, 246802 (2007). doi:10.1103/PhysRevLett.99.246802 Medline

10. A. V. Shytov, M. I. Katsnelson, L. S. Levitov, Vacuum polarization and screening of supercritical impurities in graphene. *Phys. Rev. Lett.* **99**, 236801 (2007). doi:10.1103/PhysRevLett.99.236801 Medline

11. A. H. Castro Neto, F. Guinea, N. M. R. Peres, K. S. Novoselov, A. K. Geim, The electronic properties of graphene. *Rev. Mod. Phys.* **81**, 109 (2009). doi:10.1103/RevModPhys.81.109

12. K. S. Novoselov *et al*., Two-dimensional gas of massless Dirac fermions in graphene. *Nature* **438**, 197 (2005). doi:10.1038/nature04233 Medline

13. Y. Zhang, Y. W. Tan, H. L. Stormer, P. Kim, Experimental observation of the quantum Hall effect and Berry's phase in graphene. *Nature* **438**, 201 (2005). doi:10.1038/nature04235 Medline

14. Y. Wang *et al*., Mapping Dirac quasiparticles near a single Coulomb impurity on graphene. *Nat. Phys.* **8**, 653 (2012). doi:10.1038/nphys2379

15. X. Li *et al*., Large-area synthesis of high-quality and uniform graphene films on copper foils. *Science* **324**, 1312 (2009). doi:10.1126/science.1171245

16. C. R. Dean *et al*., Boron nitride substrates for high-quality graphene electronics. *Nat. Nanotechnol.* **5**, 722 (2010). doi:10.1038/nnano.2010.172 Medline

17. R. Decker *et al*., Local electronic properties of graphene on a BN substrate via scanning tunneling microscopy. *Nano Lett.* **11**, 2291 (2011). doi:10.1021/nl2005115 Medline

18. J. Xue *et al*., Scanning tunnelling microscopy and spectroscopy of ultra-flat graphene on hexagonal boron nitride. *Nat. Mater.* **10**, 282 (2011). doi:10.1038/nmat2968 Medline

19. Supplementary materials are available on *Science* Online.

20. Y. Zhang *et al*., Giant phonon-induced conductance in scanning tunnelling spectroscopy of gate-tunable graphene. *Nat. Phys.* **4**, 627 (2008). doi:10.1038/nphys1022

21. V. W. Brar *et al*., Observation of carrier-density-dependent many-body effects in graphene via tunneling spectroscopy. *Phys. Rev. Lett.* **104**, 036805 (2010). doi:10.1103/PhysRevLett.104.036805 Medline

22. E. J. Heller, M. F. Crommie, C. P. Lutz, D. M. Eigler, Scattering and absorption of surface electron waves in quantum corrals. *Nature* **369**, 464 (1994). doi:10.1038/369464a0

23. T. Ando, Screening effect and impurity scattering in monolayer graphene. *Phys. Soc. Japan* **75**, 074716 (2006). doi:10.1143/JPSJ.75.074716

24. E. H. Hwang, S. Das Sarma, Dielectric function, screening, and plasmons in two-dimensional graphene. *Phys. Rev. B* **75**, 205418 (2007). doi:10.1103/PhysRevB.75.205418

25. V. N. Kotov, B. Uchoa, V. M. Pereira, F. Guinea, A. H. Castro Neto, Electron-electron interactions in graphene: Current status and perspectives. *Rev. Mod. Phys.* **84**, 1067 (2012). doi:10.1103/RevModPhys.84.1067

26. J. Li, W.-D. Schneider, R. Berndt, Local density of states from spectroscopic scanning-tunneling-microscope images: Ag(111). *Phys. Rev. B* **56**, 7656 (1997). doi:10.1103/PhysRevB.56.7656

27. C. Wittneven, R. Dombrowski, M. Morgenstern, R. Wiesendanger, Scattering states of ionized dopants probed by low temperature scanning tunneling spectroscopy. *Phys. Rev. Lett.* **81**, 5616 (1998). doi:10.1103/PhysRevLett.81.5616

28. W. Chen, V. Madhavan, T. Jamneala, M. F. Crommie, Scanning tunneling microscopy observation of an electronic superlattice at the surface of clean gold. *Phys. Rev. Lett.* **80**, 1469 (1998). doi:10.1103/PhysRevLett.80.1469

29. K. Morgenstern, K.-F. Braun, K.-H. Rieder, Direct imaging of Cu dimer formation, motion, and interaction with Cu atoms on Ag(111). *Phys. Rev. Lett.* **93**, 056102 (2004). doi:10.1103/PhysRevLett.93.056102 Medline

30. J. Repp *et al*., Substrate mediated long-range oscillatory interaction between adatoms: Cu /Cu(111). *Phys. Rev. Lett.* **85**, 2981 (2000). doi:10.1103/PhysRevLett.85.2981 Medline

31. M. X. Open, at www.openmx-square.org/.

32. K. T. Chan, J. B. Neaton, M. L. Cohen, First-principles study of metal adatom adsorption on graphene. *Phys. Rev. B* **77**, 235430 (2008). doi:10.1103/PhysRevB.77.235430

33. D. C. Elias *et al*., Dirac cones reshaped by interaction effects in suspended graphene. *Nat. Phys.* **7**, 701 (2011). doi:10.1038/nphys2049

34. M. van Schilfgaarde, M. I. Katsnelson, First-principles theory of nonlocal screening in graphene. *Phys. Rev. B* **83**, 081409 (2011). doi:10.1103/PhysRevB.83.081409

35. R. Geick, C. H. Perry, G. Rupprecht, Normal modes in hexagonal boron nitride. *Phys. Rev.* **146**, 543 (1966). doi:10.1103/PhysRev.146.543

36. K. K. Kim *et al*., Synthesis and characterization of hexagonal boron nitride film as a dielectric layer for graphene devices. *ACS Nano* **6**, 8583 (2012). doi:10.1021/nn301675f Medline

37. D. S. Novikov, Elastic scattering theory and transport in graphene. *Phys. Rev. B* **76**, 245435 (2007). doi:10.1103/PhysRevB.76.245435

Acknowledgments: Research supported by the Office of Naval Research Multidisciplinary University Research Initiative (MURI) award no. N00014-09-1-1066 (graphene device preparation, characterization and imaging), by the Director, Office of Science, Office of Basic Energy Sciences of the U.S. Department of Energy under contract no. DE-AC02-05CH11231 (STM instrumentation development and spectroscopy), by the NSF award nos. EEC-0832819 (*dI*/*dV* simulations) and DMR10-1006184 (DFT calculations), and by EPSRC grant EP/G036101/1 (Dirac eqn. calculations). Computational resources were provided by DOE at the LBNL NERSC facility.